Int. J. Electrochem. Sci., 11 **(2016)** 3238 - 3259

International Journal of
ELECTROCHEMICAL
SCIENCE
www.electrochemsci.org

A Novel Study on Separate and Combined Effects of the Cathodic Protection and Elastic Stress on Corrosion Behaviors of the Q235B Steel in 3.5% NaCl Aqueous Solution

Hong-Qi Yang, You Wang, San-Shan Tu, Yi-Min Li, Yi Huang[*]

School of Naval Architecture, Dalian University of Technology, Dalian 116024, Liaoning, China
[*]E-mail: huangyi@dlut.edu.cn

Received: 3 December 2015 / *Accepted:* 21 December 2015 / *Published:* 1 March 2016

The separate and combined effects of cathodic protection potential and macro-elastic stress on corrosion behaviors of Q235B steel in an aerated 3.5% NaCl aqueous solution were investigated through measurements of corrosion potential, potentiodynamic polarization characteristics, potentiostatic current and electrochemical impedance spectra (EIS). Thermodynamic and kinetic analyses as well as experimental results show that the surface energy increment due to the elastic stress is sufficient to cause the negative direction shifted of the corrosion potential and enhance the corrosion rate of the steel significantly. The transfer resistance (R_{ct}) with different elastic stress levels and various cathodic polarization potentials was obtained by fitting the EIS data with the software ZSimpWin. The relationship between R_{ct} and cathodic polarization potential under different stress levels was also investigated. In the cathodic polarization region, both the optimum protection potential (E_{opt}) and hydrogen evolution potential (E_H) could be determined by the relationship curves of R_{ct} and cathodic polarization potential. The results indicate that R_{ct} decreases significantly with increasing of elastic stress, particularly near the optimum protection potential, and also the optimum protection potential decreases linearly with the increasing of elastic stress. Some concluding remarks achieved in this study provide important recommendations that the corrosion enhancement due to the elastic stress on structural surface should be considered in safety design of marine structures, and meanwhile provide an insight into the optimization of cathodic protection system design.

Keywords: Q235B steel; Cathodic protection; EIS; Effects of stress on corrosion behaviors.

1. INTRODUCTION

Impressed-current cathodic protection (ICCP) system has been widely used as a general anticorrosion method for ships and marine structures and other metallic structures to provide protection

in regions where the coating has been damaged [1, 2]. The primary principle of ICCP is by impressing an external current on the protected structures, which can force the potential of protected structures down to the immune region. Under cathodic protection (CP), the potential becomes more negative and the corrosion rate of metals decreases with the increase of cathodic polarization current [3]. The design of cathodic protection potential usually depends on the past experience and finite empirical formulas suited for a relatively narrow range of conditions. One criterion for CP implementation is that the potential of the protected ships and marine structures (i.e., the cathode) shall be −0.80 V or more negative values measured with a silver/silver chloride (Ag/AgCl) reference electrode, or equivalent potential with other reference cells [4]. Cathodic polarization curves are usually considered as being useful in assessing the current density required for CP, especially if cathodic process controls the corrosion reactions. Therefore, in order to achieve the required protection of the ships and marine structures by employing ICCP, it is critical to obtain the precise cathodic polarization curves which are applicable for the specific marine application environment and ensure that the polarization potential can meet the CP requirement.

Ships and marine structures are usually subjected to the combined effect of mechanical and electrochemical actions when they are in service, stress or strain which can be caused by machining, operating force, welding, and cold working etc. is also unavoidable. The both mechanical effect and chemical effect interacting with each other can accelerate the failure of structural components. This synergistic effect has been defined as the mechanochemical effect (MCE) [5]. Although there have been some investigations on MCE, regrettably, most of previous studies generally focused exclusively on the effects of stress level on corrosion behaviors, and still little attention has been paid on the effects of the interaction between CP and stress on the electrochemical properties of metals in marine environment.

Melchers et al. [6] studied the corrosion behaviors of steel plates with pre-existing rusts subjected to high levels of tensile strain, and it was found that a significant damage to the rust layers would be caused just by the tensile strains which were near and beyond the elastic limit of the steel. Yang et al. [7] studied the effects of stress on corrosion behavior of metals by employing slow strain rate tests (SSRT) and electron microscopy scanning, and it was found that corrosion resistance of SAF2205 duplex stainless steel decreased slightly with increasing of elastic stress level, however corrosion resistance of pre-strained SAF2205 duplex stainless steel decreased noticeably with increasing of pre-strained level. Lin et al. [8] found that the corrosion resistance of Al-Cu-Mg alloy decreased significantly with the increasing of the applied stress in the 3.5% NaCl solution. Wang et al. [9, 10] investigated the effects of stress and stray current on corrosion behaviors of API X65 and X80 steels in alkaline solution through measurements of corrosion potential and potentiodynamic polarization characteristics, and it was found that with the increasing of applied tensile stress, the corrosion potential with and without stray current of X65 and X80 steels all shifted negatively, and meanwhile the corrosion current density increased significantly. Gao et al. [11] reported that the free corrosion potentials of the steel plate shifted in negative direction under the loading conditions, and meanwhile the mass loss of the testing steel plate was different due to stress levels, thereby it was concluded that the applied stress would accelerate the corrosion process. A similar phenomenon has been observed by Jingli Luo's and Jing Liu's groups [12, 13]. A study by Ren et al. [5] showed that the

relation between elastic stress and electrochemical effect was nonlinear through electrochemical experiments. Zhang et al. [14] investigated the effect of loading conditions on the corrosion behavior of the low carbon and low alloy steel and found that more serious damage occurred on the testing steel plate under a dynamic loading condition than that under a static loading condition because the dynamic strain led to a decrease in the protective ability of the corrosion product film on the testing steel plate. These results indicated that MCE could significantly affect the polarization characteristics, and could cause an increase of corrosion rate and a negative direction shifted of the corrosion potential. In this case, in order to provide a more efficient protection for ships and marine structures, it would be necessary to design an optimized ICCP system based on the precise analysis of corrosion characteristics by considering the coupling effect of CP and stress.

In this work, the separate and combined effects of CP and macro-elastic stress on the corrosion behaviors of Q235B steel in an aerated 3.5% NaCl solution were investigated and quantified through measurements of corrosion potential, potentiodynamic polarization characteristics, potentiostatic current and electrochemical impedance spectra (EIS). The effect of axial tensile stress on the electrochemical properties of the Q235B steel plate under various cathodic protection potentials was first examined. Then, within the corrected potential range for CP, the optimum cathodic protection potential under various stress levels was also analyzed and determined. It is anticipated that some concluding remarks achieved in this study would provide important recommendations that the general corrosion enhancement due to the elastic stress on structural surface should be considered in safety design of marine structures, and meanwhile provide an insight into the optimization of cathodic protection system design.

2. EXPERIMENTAL PROCEDURES

2.1. Specimen and solution

Test specimens used in this study were cut from a Q235B steel plate with the chemical composition as shown in Table 1.

Table 1. Chemical composition of the Q235B steel specimen.

Element	C	Si	Mn	P	S	Cu	Ni	Cr	B	Als
Content (wt.%)	0.182	0.06	0.2	0.016	0.0063	0.029	0.008	0.027	0.0002	0.0164

The yield and tensile strengths of the steel are 336.1 and 476.7 MPa, respectively, and they were determined through tensile tests in air, as shown in Fig. 1. Tensile tests were carried out by employing a 30 ton static load capacity electro-hydraulic servo controlled Shimadzu fatigue testing machine (model: EFH-2M200KN-40L) with the load speed of 3 MPa/s at the room temperature of 298 K.

Small specimens (cross-section:10 mm × 10 mm) were processed through Wire cut Electrical Discharge Machining (WEDM) from the Q235B steel plate for metallographic observations.

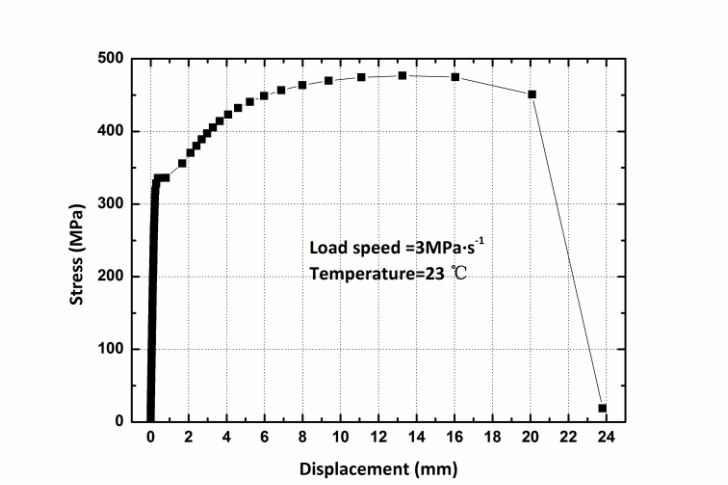

Figure 1. Typical stress–displacement curve of the Q235B steel. The yield strength is 336.1 MPa and the tensile strength is 476.7 MPa.

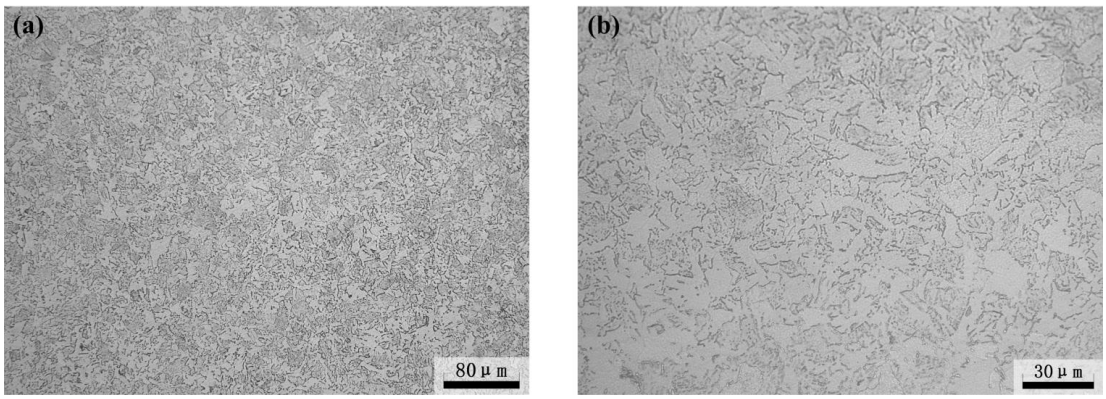

Figure 2. The representative metallographic images of the selected Q235B steel: (a) 200 times magnification; (b) 500 times magnification.

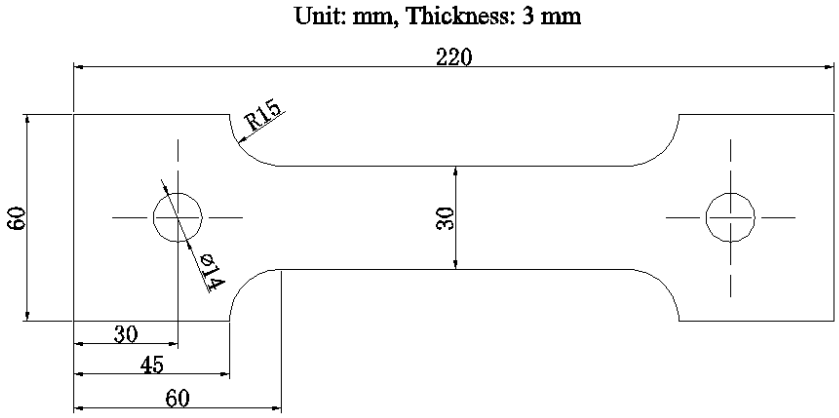

Figure 3. Schematic diagram of Q235B steel specimen for electrochemical measurements.

The specimens were first mounted with resin suitably, then abraded with silicon carbide papers up to 1000 grit and subsequently polished up to 1.5 μm diamond polishing paste employing standard metallographic techniques, and finally were etched with 3% nital for revealing the microstructures. These were examined by using an optical microscope (model: Leica, MEF4A) which revealed the microscopic structure to contain predominantly the ferrite and pearlite. The representative metallographic microstructure of the selected Q235B steel is as shown in Fig. 2.

The dog-bone-shaped specimens were fabricated and used in electrochemical measurements, with the dimension as shown in Fig. 3. Prior to each electrochemical test, all the specimens were first ground with silicon carbide papers to a grit finish of #1000 and then thoroughly cleaned by dehydrated ethanol. The specimens were subsequently in contact with an experimental apparatus and the area of the specimen exposed to the test solution during the long time electrochemical measurements was kept invariant and equaled to 1 cm^2.

All the electrochemical tests were carried out in the same 3.5% NaCl aqueous solution. Prior to tests, the solution was continuously aerated with air bubbles for one hour to attain an oxygen saturation condition. The gas flow was maintained throughout the tests, and simultaneously, the electrolyte was held at the temperature of 25℃ by employing a thermostatic device.

2.2. Loading method

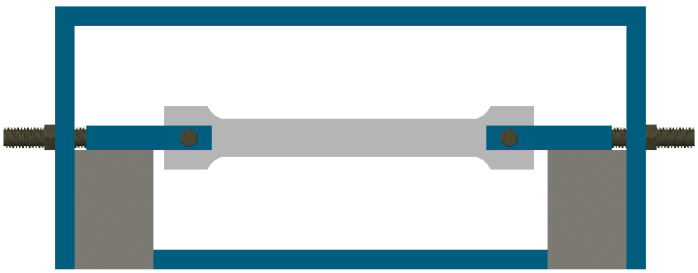

Figure 4. The uniaxial tensile loading apparatus. Different stress levels can be obtained by adjusting the adjustable bolt.

The uniaxial loading method was adopted in the present study to obtain constant tensile stress for electrochemical tests. The uniaxial tensile loading experimental apparatus is as shown in Fig. 4. Different stress levels can be obtained by adjusting the adjustable bolt. The exact value of the tensile stress was measured and calculated by a strain gauge. The levels of the elastic stress used in this study were 0 MPa, 70 MPa, 100 MPa, 130 MPa and 160 MPa (nearly 50% of Yield strength), respectively.

2.3. Electrochemical measurements

For the investigation of effects of the elastic stress on general corrosion behaviors of the Q235B steel, electrochemical measurements, including corrosion potential, potentiodynamic polarization characteristics, potentiostatic current and EIS, were performed by using a PAR 263A

potentiostat in the conventional three-electrode cell system, as shown in Fig. 5, where the Q235B steel specimen was used as the working electrode, a silver/silver chloride electrode (Ag/AgCl, 3.5M KCl) was used as the reference electrode and a platinum net (area of 4 cm^2) was used as the counter electrode. A general view of the experimental device for electrochemical measurements on the tensile specimen is as shown in Fig. 6.

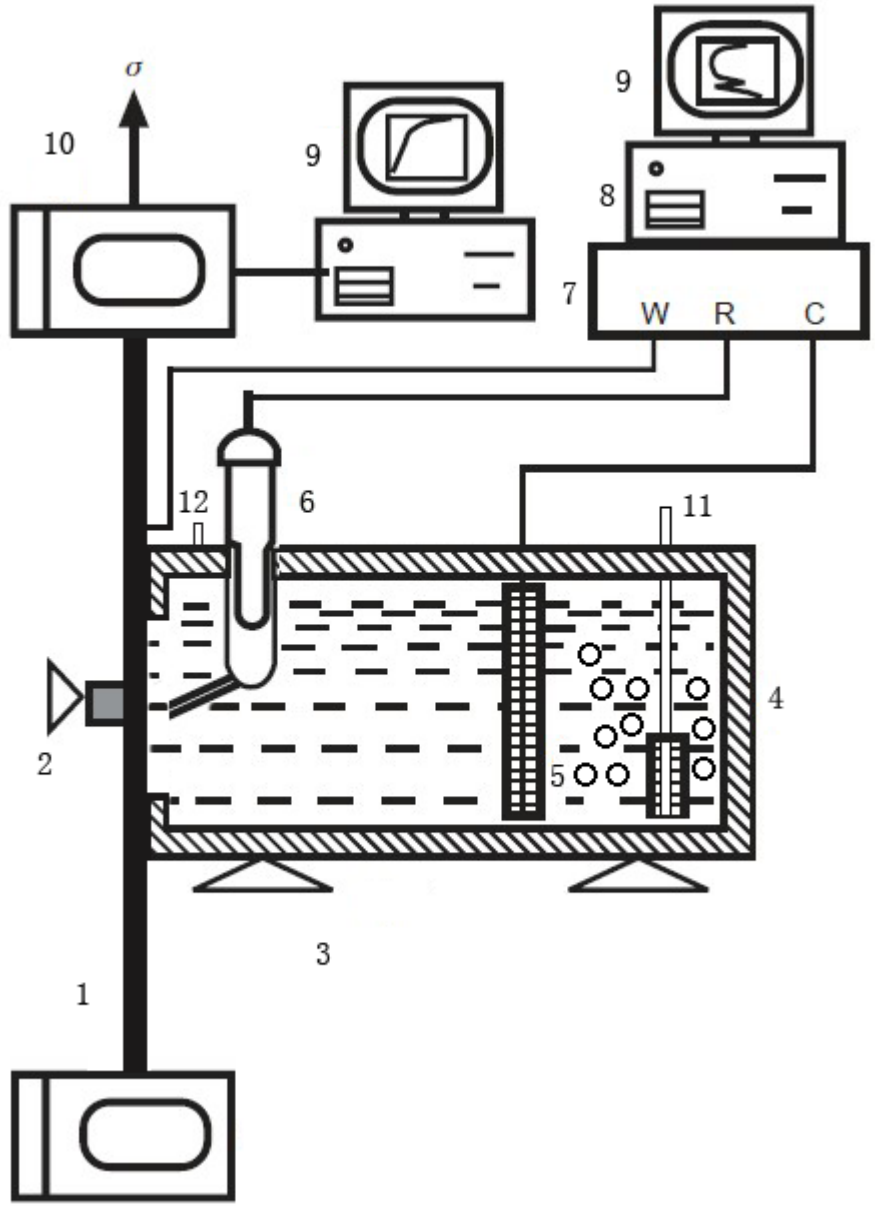

Figure 5. Schematic diagram of the experimental setup for electrochemical measurements on the tensile specimen. 1 – specimen, 2 –clamping screw, 3 – supports, 4 – glass container filled with electrolyte, 5 – platinum net, 6 – Ag/AgCl electrode, 7 – PAR 263A potentiostat, 8 –5210 Frequency Response Analyzer, 9 – computer, 10 – loading apparatus with a strain gauge, 11 – oxygen, 12 – outlet for oxygen.

To investigate the effect of elastic stress on corrosion potential, the curves of free corrosion potential vs. time for the Q235B steel under various elastic stress levels were measured for 12 hours. Prior to the measurements of potentiodynamic polarization characteristics, specimens under various stress levels were immersed in the electrolyte at the open circuit potential (OCP) for 12 hours to reach a steady state. The potentiodynamic polarization characteristics were obtained by scanning the potential range from -250 mV (vs. OCP) to +250 mV (vs. OCP) at a scanning rate of 0.166 mV/s. Some degree of specimen roughening could occur with each potentiodynamic polarization; therefore, new test specimens were used for the repeated potentiodynamic polarizations. The potentiostatic current measurements of Q235B steel under different stress levels were carried out in the potential range of -0.6 $V_{Ag/AgCl}$ to -1.1 $V_{Ag/AgCl}$.

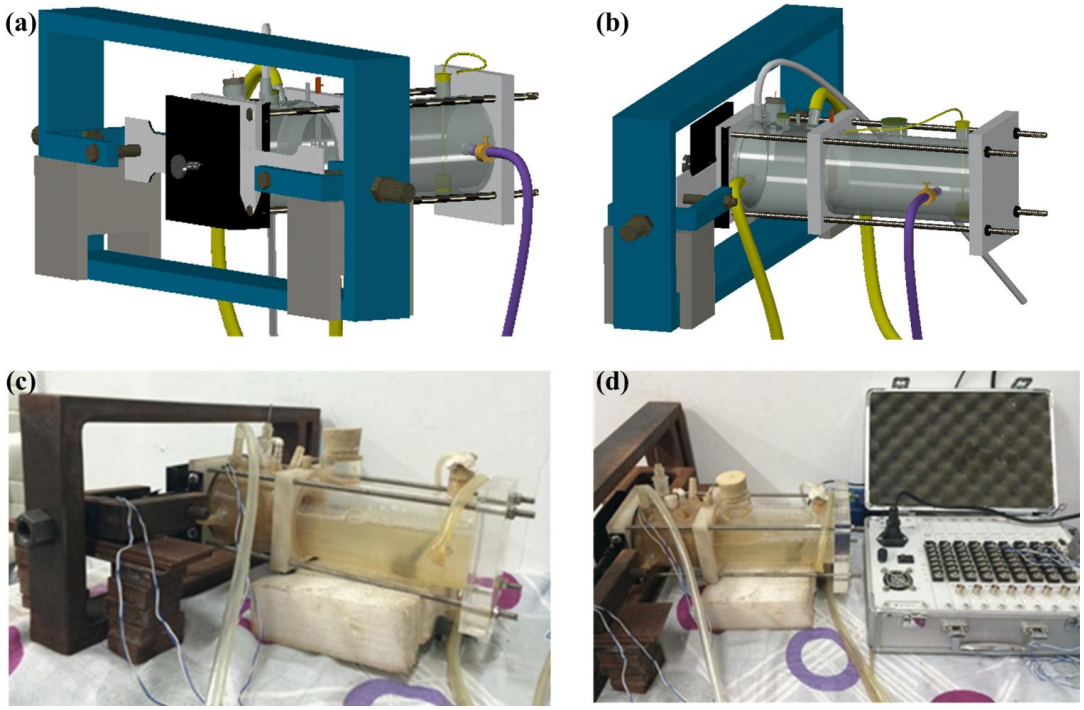

Figure 6. A general view of the experimental device for electrochemical measurements on the tensile specimen: (a) and (b) are the left and right views for 3D model diagrams, respectively; (c) and (d) are the actual photographs.

The quantitative determination of stress effect in cathodic protection was realized by employing EIS technique. EIS diagrams were measured by employing the PAR 263A potentiostat coupled with a 5210 Frequency Response Analyzer with the AC disturbance signal of 10mV in the frequency range from 100 kHz to 10 mHz. The extent of polarization of the EIS was small, so the change in surface morphology of test specimens could be neglected. To eliminate the influence of the microstructure changes of different test specimens on the results of electrochemical measurements, the same specimen under different stress levels was used to study the EIS characteristics in the potential range of -0.6 $V_{Ag/AgCl}$ to -1.2 $V_{Ag/AgCl}$.

3. RESULTS

3.1. Corrosion potential measurements

The corrosion potential measurements of the Q235B steel specimens under different stress levels in the 3.5% NaCl aqueous solution were conducted through the specimens placed in the uniaxial loading apparatus together with the electrochemical test device.

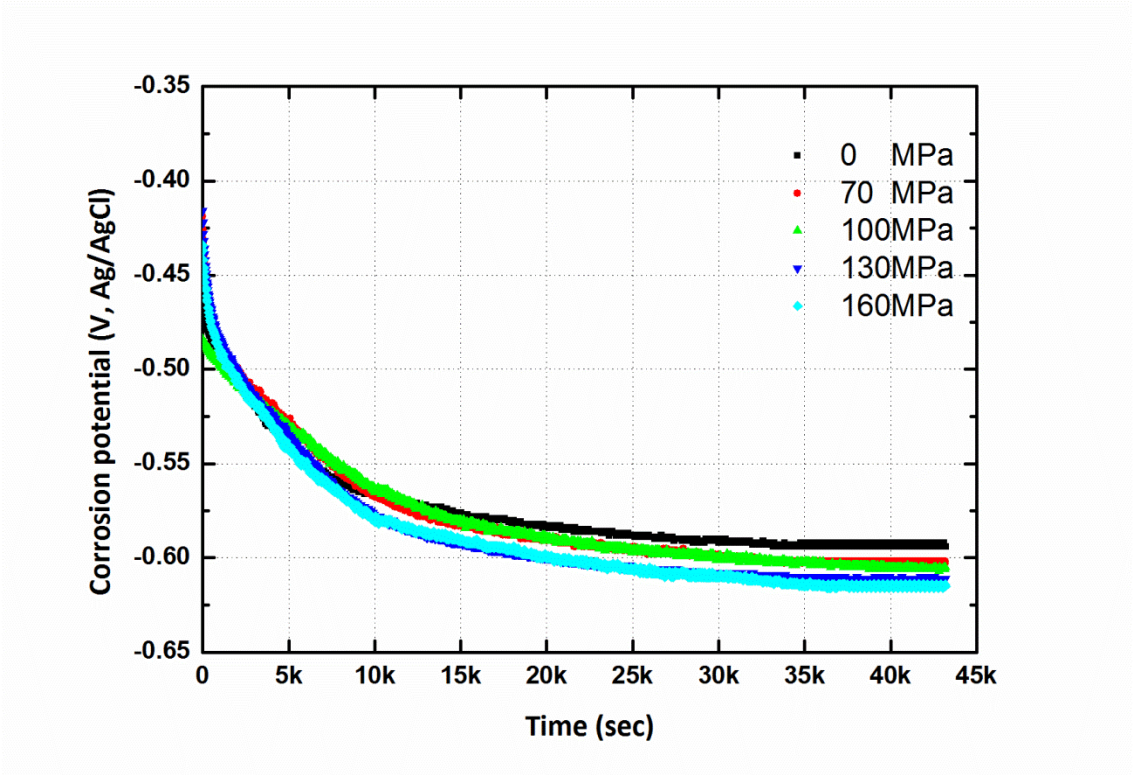

Figure 7. Time dependence of corrosion potentials of the specimen under various stress level.

Fig. 7 shows the time dependence of corrosion potential for the specimens under different stress levels in the 3.5% NaCl aqueous solution. It can be seen that corrosion potential of the loading-free specimen decreased gradually and approached a relatively steady-state value of -0.594 V vs. Ag/AgCl. Compared with the former, corrosion potentials of the specimens under the loading condition decreased more quickly and reached a slightly more negative value. With the increasing of stress level, there was a marked negative shift for corrosion potential, with the variation about tens of millivolts within the applied elastic stress range, comparing with the loading-free specimen.

According to the mechanochemical theory [15], the value of the electrode potential is directly related to the corrosion tendency of materials. The higher the electrode potential is, the lower the corrosion tendency will become. This result illustrated that during the initial stage of immersion, the specimen under the loading condition underwent a more serious attack, which could be relate to the enhanced surface reactions, and also corroded more severely as stress level increased.

3.2. Potentiodynamic polarization characteristics measurements

After the Q235B steel specimens under different elastic stress levels were immersed in the electrolyte for 12 hours, the potentiodynamic polarization characteristics were measured and are as shown in Fig. 8.

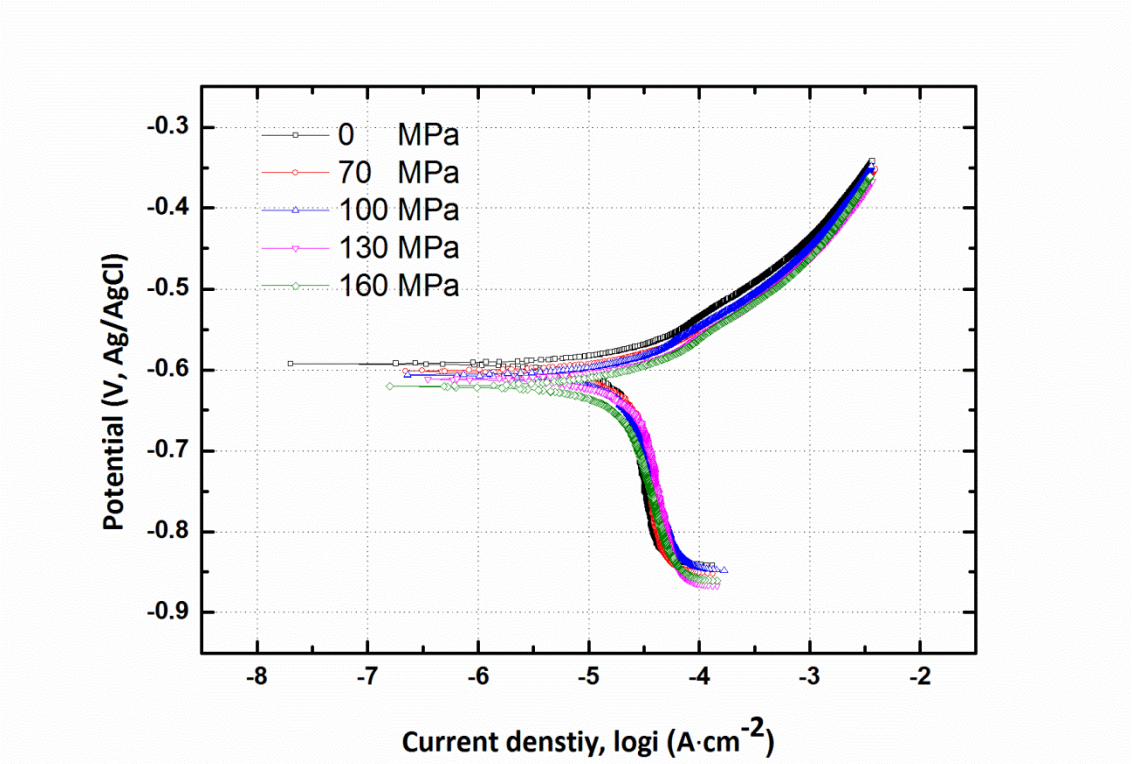

Figure 8. Evolution of Tafel polarization characteristics under various stress levels in the 3.5% NaCl aqueous solution.

It can be seen that the polarization curves have shifted significantly, i.e., the applied loads influenced the polarization characteristics of the specimens. As shown in Fig. 8, with the increasing of elastic stress level, the free corrosion potential shifted in the negative direction, as indicated by the above measurements of corrosion potential under different stress levels. Moreover, it can be noted that anodic polarization curves just shifted downwardly without intersections, while in the potential range of cathodic polarization, the cathodic polarization characteristics changed: when the potential was above -0.7 V vs. Ag/AgCl, the cathodic current density decreased gradually along with the increasing of stress level; however, for the specimen at the potential below -0.7 V vs. Ag/AgCl, the cathodic current density increased with the increase of stress level.

3.3. Potentiostatic current density measurements

Fig. 9 shows an example of the time dependence of cathodic current density of the loading-free and loaded specimens potentiostatically polarized at the protection potential of −0.9 V vs. Ag/AgCl.

For the loading-free specimens, cathodic current density shifted negatively first and then increased to reach a relatively steady value of 52.5 μA/cm^2.

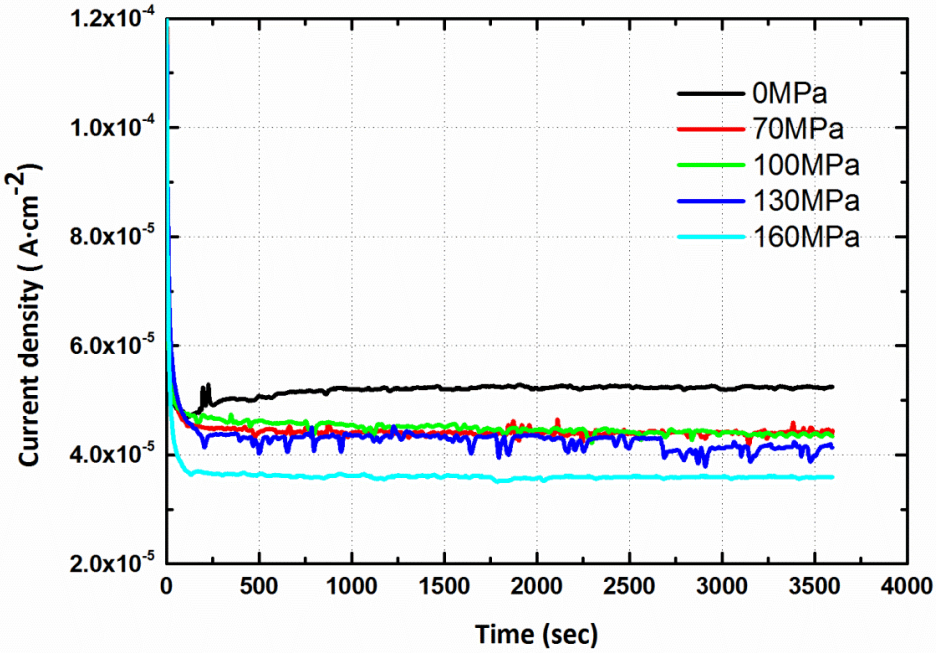

Figure 9. Time dependence of current densities of the loading-free and loaded specimens potentiostatically polarized at −0.9 V vs. Ag/AgCl.

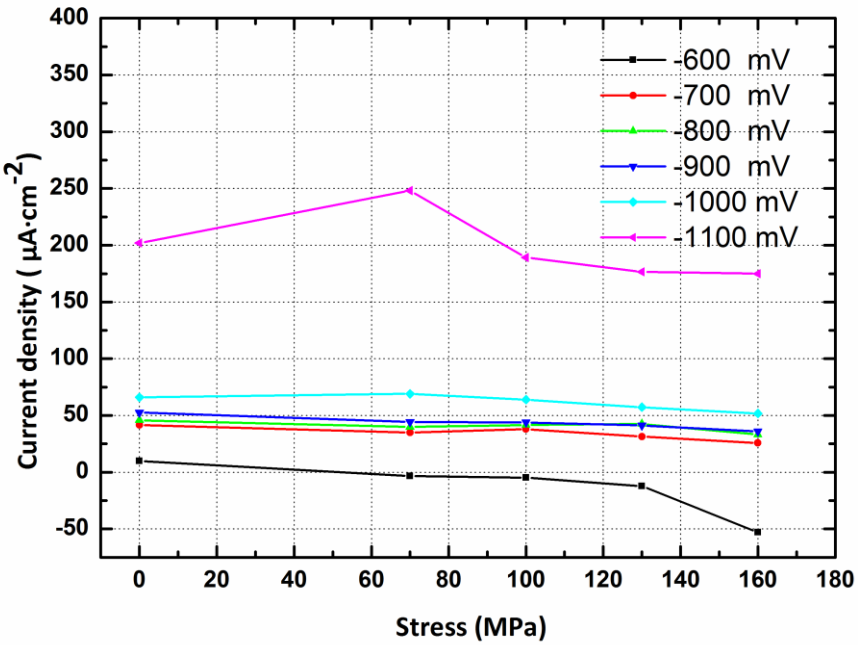

Figure 10. The steady-state impressed current density of the Q235B steel polarized at different potentials under various stress levels.

There were similar features for all loaded specimens, i.e., cathodic current density decreased gradually and approached a steady state. It is apparent that the cathodic current density decreased more quickly with the increasing of stress level. Furthermore, the changing trends of the steady-state impressed current density of the Q235B steel specimens polarized at various potentials with the increasing stress level were plotted in Fig. 10. It can be noted that, for the specimens at the potential of -0.6 V vs. Ag/AgCl, as the elastic stress increased, entering the stress range of 0 MPa to 70 MPa, the current density showed an obvious change from positive to negative, which indicated that the applied elastic stress caused the free corrosion potential to decrease to the potential relatively negative than -0.6 V vs. Ag/AgCl, consequently, the stressed specimens in the range of 70 MPa to 160 MPa were actually in anodic polarization state as the polarization potential was equal to -0.6 V vs. Ag/AgCl. The changing trend of current density with elastic stress for the Q235B steel specimens at the relatively negative potential of -0.7 $V_{Ag/AgCl}$ to -0.8 $V_{Ag/AgCl}$ was coincident with that polarized at the potential of -0.9 V vs. Ag/AgCl. For more negative potential ranging from -1.0 $V_{Ag/AgCl}$ to -1.1 $V_{Ag/AgCl}$, the cathodic current density increased first and then decreased with the increasing of stress level. Therefore, it would be necessary to adjust the impressed cathodic current supply to keep the Q235B steel under various stress levels maintain a relatively constant potential, especially for some critical potential. For example, for the critical cathodic protection potential of -1.1 V vs. Ag/AgCl, if apply the current density suited for loading-free Q235B steel to the loaded Q235B steel, it might result in the possible risk of hydrogen embrittlement.

3.4. EIS measurements

The EIS data were fitted with the software ZSimpWin to equivalent circuits applicable for modeling at various potentials and stress levels. Fig. 11 shows the EIS plots measured on Q235B steel specimens under different stress levels in the potential range of -0.6 $V_{Ag/AgCl}$ to -1.2 $V_{Ag/AgCl}$ after reaching a stable state in the 3.5% NaCl solution. It can be seen that there were similar impedance characteristics for all the test specimens, i.e., one depressed semicircle over the entire frequency range, meaning that only one time constant exists on the interface between the solution and the solid specimen. When the polarization potential was kept constant and the applied elastic stress increased, taking Fig. 12 for example, there was an obvious decrease in the size of the semicircle. For the stress level ranging from 0 MPa to 130 MPa, the size of the semicircle increased firstly then decreased with the decrease of cathodic polarization potential, and reached the maximum at the potential around -0.8 $V_{Ag/AgCl}$. As the applied stress increased to 160 MPa, the potential at which the semicircle reached maximum size shifted negatively from -0.8 $V_{Ag/AgCl}$ to -0.9 $V_{Ag/AgCl}$. These results showed that both elastic stress and cathodic potential could affect the impedance characteristics of the specimen.

In order to further investigate the effects of stress level and cathodic protection potential on EIS characteristics of Q235B steel immersed in the 3.5% NaCl aqueous solution, an electrochemical equivalent circuit which contained a solution resistance, R_s, in series with a parallel circuit of charge-transfer resistance, R_{ct}, and constant phase element (CPE) for the double-charge layer, was used to fit the EIS data.

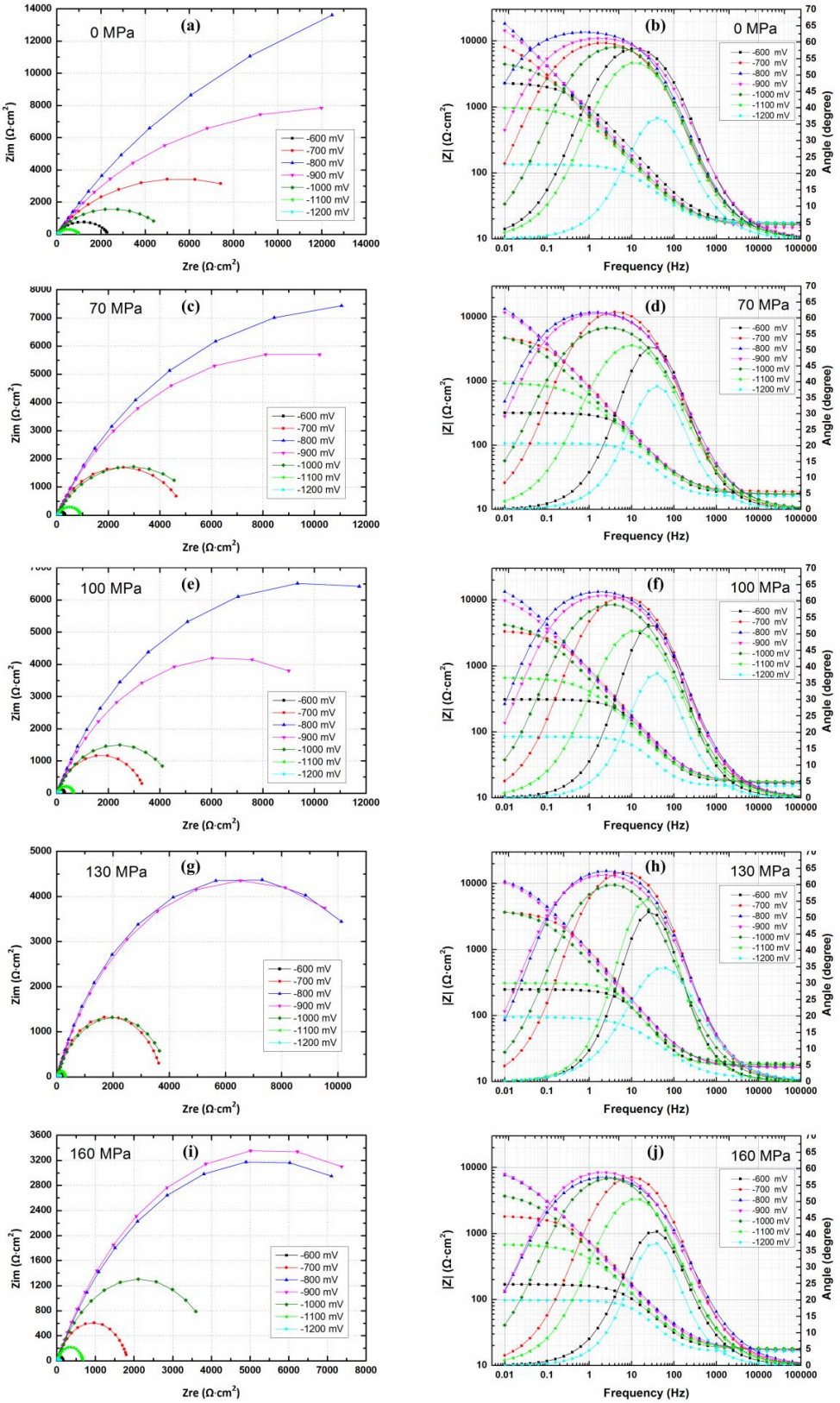

Figure 11. EIS plots measured on the various polarization specimens under different levels of stress: (a) Nyquist (0 MPa), (b) Bode (0 MPa); (c) Nyquist (70 MPa), (d) Bode (70 MPa); (e) Nyquist (100 MPa), (f) Bode (100 MPa); (g) Nyquist (130 MPa), (h) Bode (130 MPa); (i) Nyquist (160 MPa), (j) Bode (160 MPa).

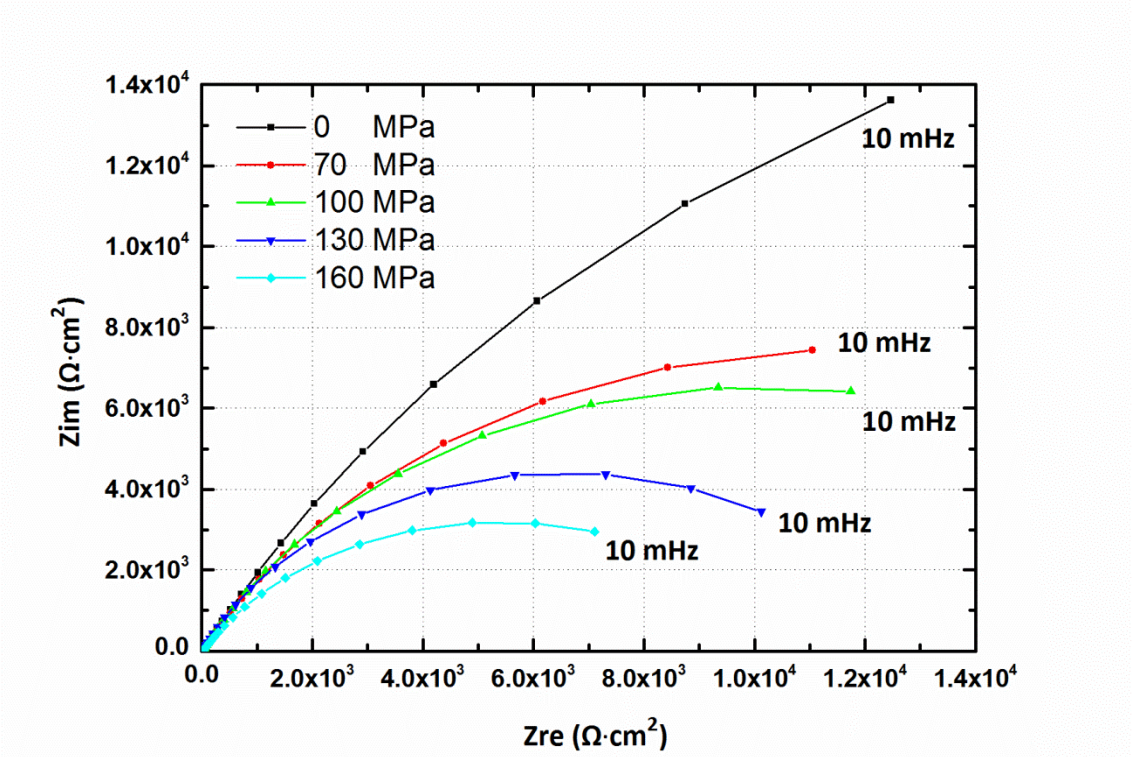

Figure 12. Nyquist diagrams measured on the Q235B steel in the 3.5% NaCl at the potential of −0.8 V vs. Ag/AgCl under different stress levels

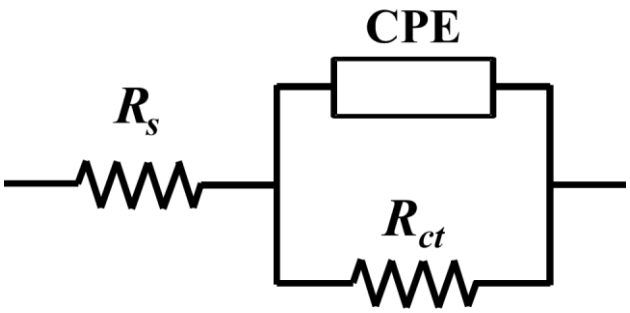

Figure 13. Equivalent circuit for the EIS data fitting, where R_s is the solution resistance, R_{ct} is the charge-transfer resistance and CPE is the constant phase element.

A non-ideal capacitive response from the corrosion system was considered by using CPE in place of a pure capacitance in the circuit, and the electrical equivalent circuit is as shown in Fig. 13. The CPE behavior was thought to be caused by the surface roughness and heterogeneities, electrode porosity, non-uniform potential and current distributions associated with electrode geometry [2, 16-22], and the impedance of a CPE is given by:

$$Z_{CPE} = \frac{1}{Q(j\omega)^{\alpha}} \qquad (1)$$

where Q is the magnitude of admittance of CPE, ω is the angular frequency (rad/s) and α is the exponential term [23]. When $\alpha = 1$, a CPE can simplify to a pure capacitor, and when $\alpha = 0$, a CPE

can simplify to a pure resistor. The similarity between the impedance relations of a capacitor and CPE make it tempting to approximate Q as a capacitance when α approaches 1, but this is an inappropriate approximation [23]. Q does not have units of capacitance, and small deviations of α from 1 can lead to large computational errors of capacitance [19, 23, 24]. A thorough description of CPE behavior is provided in Ref. [20, 21] and [23, 25, 26].

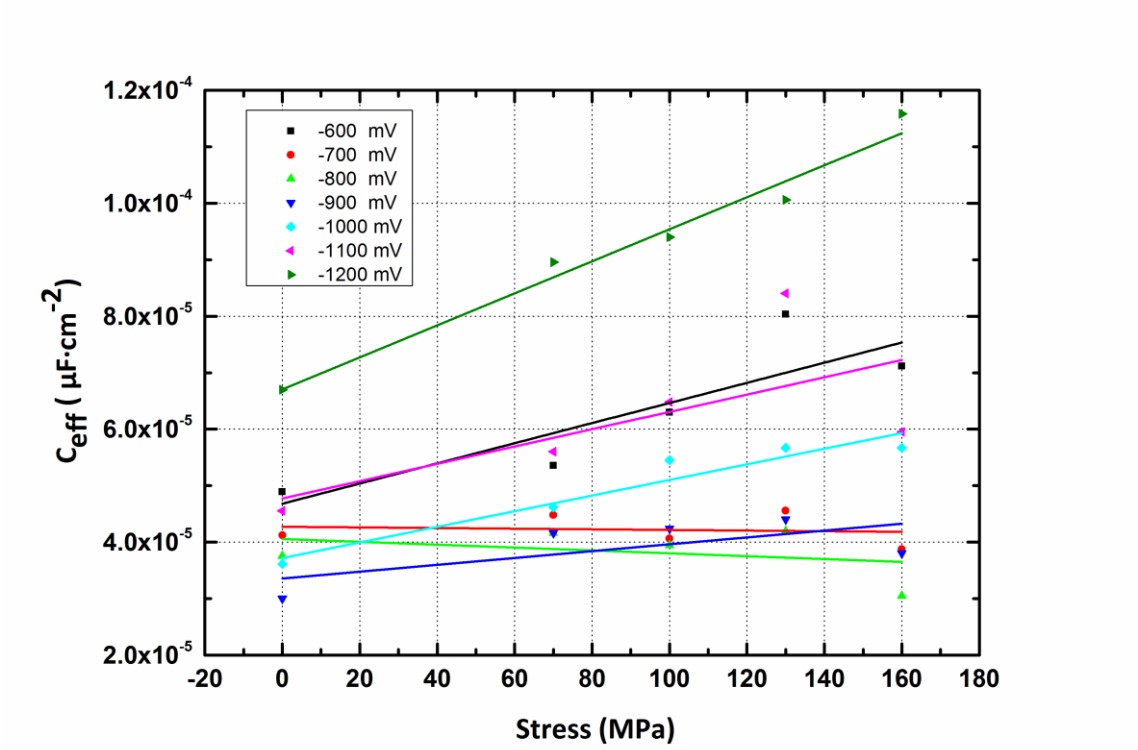

Figure 14. Fitted values of effective capacitance of constant phase element (CPE) from the impedance spectra measured on the Q235B steel polarized at various potentials under different stress levels.

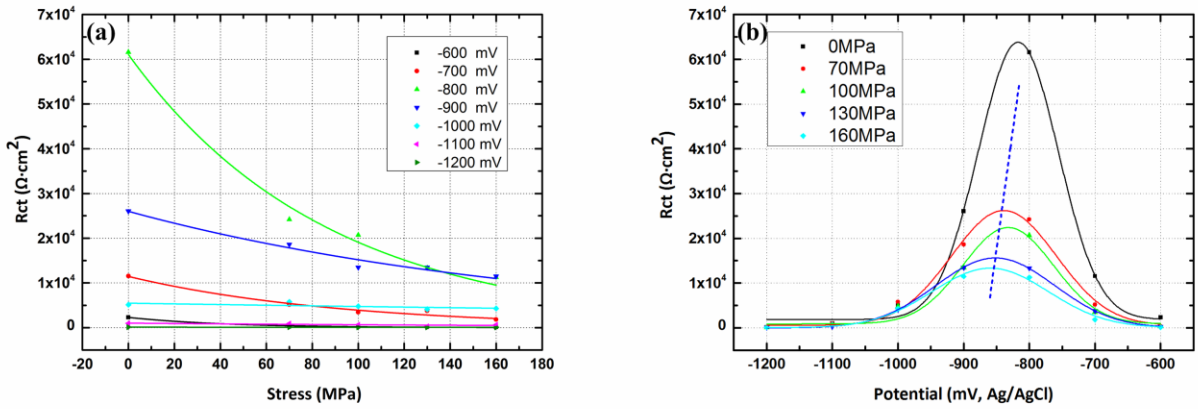

Figure 15. Fitted values of charge-transfer resistance (R_{ct}) from the impedance spectra measured on the Q235B steel polarized at various potentials under different stress levels: (a) constant potential; (b) constant stress.

The expression developed by Brug et al [21], which could be used to calculate the effective capacitance of a CPE measured through EIS, was adopted in present study. The effective capacitance (C_{eff}) was found to take the following form

$$C_{eff} = Q^{1/\alpha}\left(R_S^{-1} + R_{ct}^{-1}\right)^{(\alpha-1)/\alpha} \qquad (2)$$

Fig. 14 shows the relationships between the fitted values of C_{eff} based on the measured EIS data and the applied elastic stress as well as cathodic polarization potential, respectively.

It can be seen clearly that, when the cathodic polarization potential was kept constant, the relationship between C_{eff} and stress, independent of the applied cathodic potentials, was approximately linear. For the Q235B steel specimen at the potential of -0.6 $V_{Ag/AgCl}$**,** a significant increase of the C_{eff} value was observed as the stress increased. For relatively negative potential range of -0.7 $V_{Ag/AgCl}$ to -0.9 $V_{Ag/AgCl}$, no obvious change was noted in the value of C_{eff} with the increase of stress level, indicating that the cathodic protection potentials within the present range played their protective roles effectively and reduced the impact of stress level significantly. With the further decrease in potential range from -1.0 $V_{Ag/AgCl}$ to -1.2 $V_{Ag/AgCl}$, the C_{eff} value increased obviously with the increase of the stress level again, implying that the applied potential caused inefficient, invalid or even negative effect of the cathodic polarization potential due to the possible hydrogen evolution reaction. At the potential of -1.2 $V_{Ag/AgCl}$, a large amount of hydrogen bubbles were observed on the surface of Q235B steel. Hydrogen penetrated into specimen under the action of the electrochemical driving force and would reduce the mechanical properties of the Q235B steel. At the potential around -1.0 $V_{Ag/AgCl}$, hydrogen permeation might have occurred. Therefore, the most negative cathodic protection potential for Q235B steel in present study should be approximately equal to -1.0 $V_{Ag/AgCl}$, which was the hydrogen evolution potential.

Fig. 15 shows the fitted values of R_{ct} under different stress levels at various potentials of -0.6 $V_{Ag/AgCl}$ to -1.2 $V_{Ag/AgCl}$. The parameter R_{ct} can reflect the surface activity and corrosion resistance of the Q235B steel under different potentials and stress levels. The smaller the value of R_{ct} is, the worse its corrosion resistance and the higher its surface activity become. It can be observed that, when the cathodic polarization potential was kept constant, the value of R_{ct} decreased significantly as the stress increased, as shown in Fig. 15(a), indicating that stress could reduce the protective effect of cathodic protection, in line with the results of corrosion potential measurements, potentiodynamic polarization and potentiostatic current characteristics measurements. The EIS results verified the accuracy of the previous measurement results in present study.

In addition, a GaussAmp function, as the amplitude version of Gaussian peak function, was utilized to process the curve fitting of R_{ct} under various stress levels and cathodic polarization potentials, and the fitting results were satisfactory from the calculations of actual data and fitting-figures, as shown in Fig. 15(b). According to Fig. 15(b), within the potential range of -0.6 $V_{Ag/AgCl}$ to -0.7 $V_{Ag/AgCl}$, R_{ct} increased slowly with the decreasing of cathodic polarization potential. For relatively negative cathodic polarization potentials from -0.7 $V_{Ag/AgCl}$ to -0.85 $V_{Ag/AgCl}$, a dramatic increase of the R_{ct} value was observed with the decreasing potential. With the further decrease of the polarization potential, R_{ct} showed a significantly decreasing trend in the potential range from -0.85 $V_{Ag/AgCl}$ to -1.0

$V_{Ag/AgCl}$, and finally decreased gradually towards 0 $\Omega \cdot cm^2$ in the potential range of -1.0 $V_{Ag/AgCl}$ to -1.2 $V_{Ag/AgCl}$.

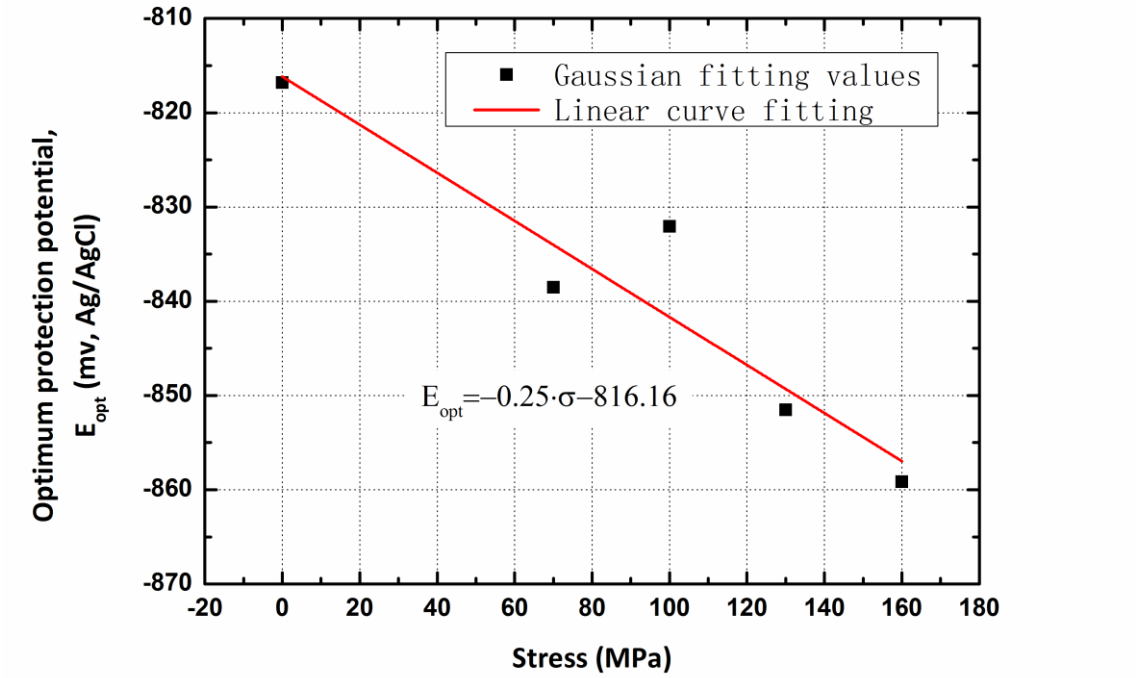

Figure 16. Dependence of the fitted optimum cathodic protection potential on the stress level.

At the same time, it can be found that the increase of elastic stress level could reduce the changing amplitude of R_{ct} with the decreasing cathodic polarization potential, and also could change the optimum cathodic protection potential where R_{ct} reached the peak value, as indicated by the blue dotted line in Fig. 15(b). Thus, in order to further quantify the effect of elastic stress on the optimum cathodic protection potential, the novel relationship between them was worth studying. The fitted optimum cathodic protection potential as a function of stress level is as shown in Fig. 16. It can be noted that the optimum cathodic protection potential was inversely proportional to the stress level, and the slope of this linear fitting equation was -0.25 mV/MPa, indicating that an enhanced impressed current would be necessary to make the cathodic protection potential decrease to the optimum protection potential with the increase of stress level for protected ships and marine structures, which could provide an insight into the optimization of cathodic protection system design in the further research work.

4. DISCUSSION

The present work demonstrated that both the applied elastic stress and the impressed-current cathodic protection potential could affect the electrochemical properties of the Q235B steel plate in the 3.5% NaCl aqueous solution.

4.1. Kinetics of corrosion behaviors of Q235B steel in 3.5% NaCl aqueous solution

The electrochemical anodic and cathodic reactions of Q235B carbon steel in the oxygenated 3.5% NaCl aqueous solution usually contain the iron oxidation and the reduction of oxygen and water, respectively:

$$\text{Anodic reaction: } Fe \rightarrow Fe^{2+} + 2e^{-} \quad (3)$$

$$\text{Cathodic reaction: } O_2 + 2H_2O + 4e^{-} \rightarrow 4OH^{-} \quad (4)$$

$$H_2O + e^{-} \rightarrow H + OH^{-} \quad (5)$$

In particular, at less negative potentials, the oxygen reduction dominates the cathodic process, while hydrogen evolution dominates at more negative potentials [3, 27]. Therefore, cathodic protection could have a great effect on the cathodic reaction process and the anodic characteristics of Q235B steel.

For a uniform corrosion system, when the electrochemical system is in a steady-state condition, according to active polarization electrochemistry [28], the corrosion potential derived from the corrosion kinetic equation can be expressed as follows:

$$\varphi_{corr} = \frac{b_a b_c}{b_a + b_c} \ln \frac{i_c^0}{i_a^0} + \frac{b_a}{b_a + b_c} \varphi_{e,c} + \frac{b_c}{b_a + b_c} \varphi_{e,a} \quad (6)$$

where φ_{corr} is the corrosion potential; i_a^0 and i_c^0 are anodic and cathodic exchange current densities, respectively; $\varphi_{e,a}$ and $\varphi_{e,c}$ are anodic and cathodic equilibrium potentials, respectively; b_a and b_c are anodic and cathodic polarization constants (Tafel slopes), respectively.

The polarization characteristics measured at the various stress levels in Fig. 8 were fitted to determine b_a and b_c respectively, and the values of b_a and b_c under various stress levels are listed in Table 2. It can be noted that the applied elastic stress almost had no significant influence on the cathodic Tafel slope, and meanwhile, with the increasing of stress level, there was only a slight increase for the anodic Tafel slope, with the variation within 6 mV/dec^{-1}.

Table 2. Fitted anodic and cathodic Tafel slopes (b_a and b_c) of Q235B steel under various stress levels in the 3.5% NaCl aqueous solution.

Stress (MPa)	0	70	100	130	160
b_a (mV/dec^{-1})	119.95	121.48	125.77	123.55	125.46
b_c (mV/dec^{-1})	259.41	285.38	241.76	282.02	246.53

Therefore, for the range of the low levels of elastic stress studied in present study, it was reasonable to consider that the values of b_a and b_c remained nearly invariant, and take their respective average. Thus, the variation of corrosion potential could be attributed to the stress-induced alteration of equilibrium potentials and exchange current densities of the anode and cathode in the electrochemical system.

4.2. Effect of static elastic stress on corrosion behaviors of Q235B steel

According to Gutman's theory [29], the change of equilibrium potential caused by external pressure can be characterized by the following equation:

$$\Delta\varphi_e = -\frac{\Delta P V_m}{zF} \qquad (7)$$

where ΔP is the hydrostatic pressure, V_m is the molar volume of the electrode material, z is the valence of metal ions and F is Faraday's constant.

Replacing the $\varphi_{e,a}$ in Eq. (6) with $(\varphi_{e,a}+\Delta\varphi_{e,a})$, and then the variation of corrosion potential can be expressed as

$$\Delta\varphi_{corr} = \frac{b_c}{b_a + b_c}\Delta\varphi_{e,a} \qquad (8)$$

Therefore, a positive hydrostatic pressure would decrease the corrosion potential of the steel, indicating an increase of the electrochemical thermodynamic activity [15].

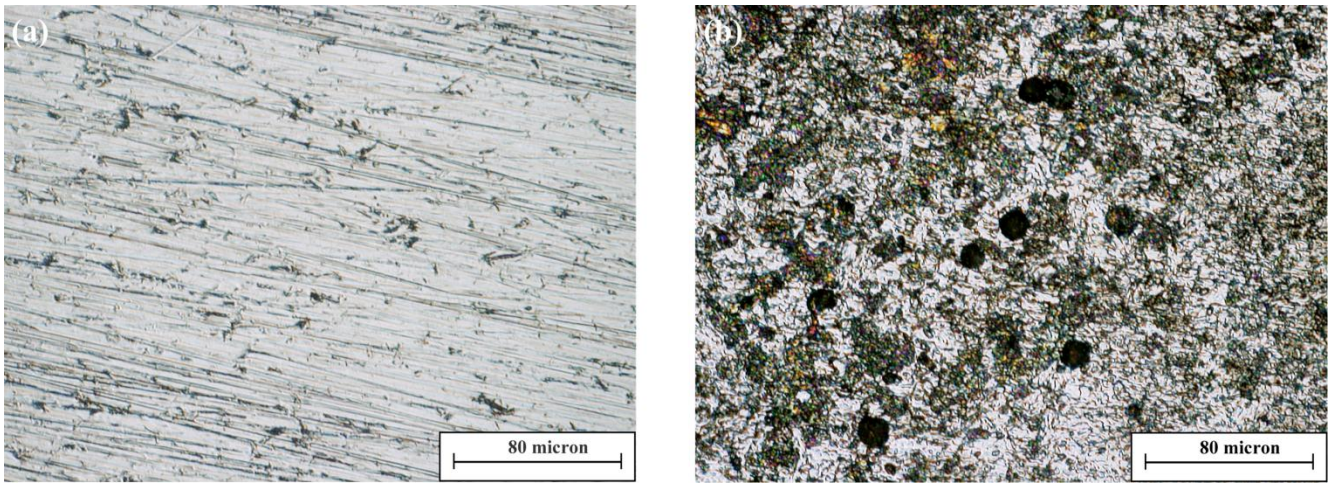

Figure 17. Micrograph of the corroded Q235B steel stressed at 160 MPa after immersion for different times and the rust was removed: (a) 0.5 h; (b) 12 h.

In this study, uniaxial stress (σ) was applied on the steel specimen, and ΔP, as the hydrostatic pressure, equals to 1/3 of the applied elastic stress [29]. For the Q235B steel, with z = 2, F =96485 C/mol, V_m ≈7.13 cm^3/mol, b_a =123.24 mV/decade and b_c =263.02 mV/decade, $\Delta\varphi_{corr}$ from unstressed to 160 MPa was calculated to be 4.03 mV, which was far smaller than the experimental value of 22 mV. The variation might result from the stress concentration at pits which were caused by the chloride ion, as shown in Fig. 17, which is the micrograph of the corroded Q235B steel stressed at 160 MPa after immersion in the 3.5% NaCl aqueous solution for different times and the rust was removed.

According to the effect of elastic stress on corrosion behaviors of steels [29], the corrosion potential difference $\Delta\varphi_{corr}$ between a loading-free electrode and the loaded electrode has a linear relationship with stress level. But also, it is worthy pointing out that a correction factor which can cover the effects of various environmental factors, such as aggressive species, solution pH, local

corrosion pits, etc., should not be ignored. And finally, Eq. (6) can be expressed as a linear approximation

$$\varphi_{corr} = \varphi_{corr}^{0} + \beta \cdot \sigma \quad (9)$$

where φ_{corr}^{0} is the corrosion potential of loading-free electrode, β is the experimental fit constant.

The mathematical formula of φ_{corr} and σ was derived through corrosion potential measurements, as shown in Fig. 18, and the values of φ_{corr}^{0} and β were -0.593 $V_{Ag/AgCl}$ and -0.137 mV/MPa, respectively.

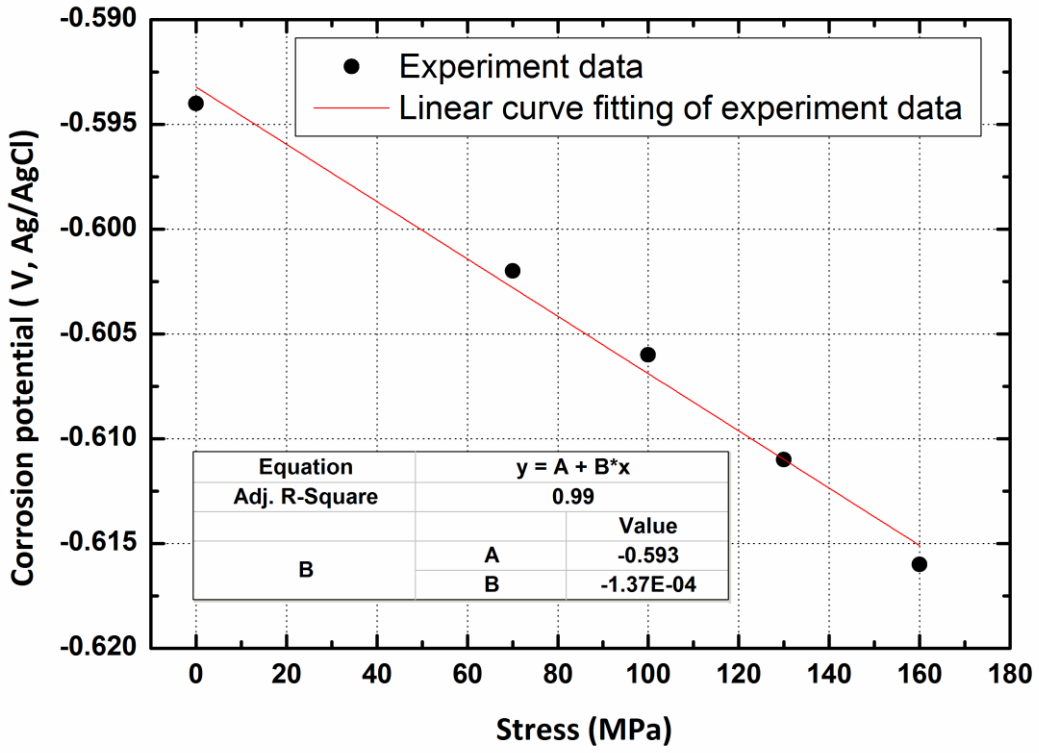

Figure 18. The changing rule of the corrosion potential for Q235B steel under various stress levels.

Therefore, if the specimen is in elastic range, the corrosion potential of the loaded specimen can be calculated by the above formula. Furthermore, overall, the calculated results were in agreement with the results of potentiodynamic and potentiostatic polarization characteristics measurements in terms of the free corrosion potential impacted by stress level. Taking the Fig. 15(a) for example, where the values of R_{ct} were fitted through the impedance spectra measured at various potentials from -0.6 $V_{Ag/AgCl}$ to -1.2 $V_{Ag/AgCl}$, it can be seen from the EIS measurement that the applied elastic stress could affect obviously the electrochemical properties of the Q235B steel as the steel was polarized at some cathodic protection potentials.

4.3. Effect of cathodic polarization potential on corrosion behaviors of Q235B steel

Q235B steel under cathodic protection by employing the impressed current can be prevented from oxidizing. Nevertheless, as the potential becomes too negative, which is called overprotection, the protective effects of cathodic protection on steel would reverse, resulting in the deteriorated mechanical properties of the Q235B steel, and also waste energy.

The effects of cathodic protection potential on corrosion behaviors of the Q235B steel as well as the change of optimization cathodic protection potential with stress level were investigated with the charge transfer resistance.

The EIS measurements on both loading-free (Fig. 11(a-b)) and loaded (Fig. 11 (c-j)) Q235B steel specimens at various cathodic polarization potentials show only one semicircle existing in the low frequency range. It can be seen that the impedance values at high frequency domain, which are associated with the corrosion product layer deposited on the surface of Q235B steel, were nearly the same, whereas those at the low frequency domain related to the interfacial charge-transfer reaction changed obviously. The charge transfer resistance of the impedance, R_{ct}, depends on both the transfer resistance of anodic reaction and that of cathodic reaction. In the near-neutral pH 3.5% NaCl aqueous solution, given that the cathodic reaction was dominated by the dissolved oxygen diffusing to the steel surface, the transfer resistance of cathodic reaction, $R_{ct,c}$, decreases slowly with the decreasing of the cathodic polarization potential, whereas the transfer resistance of anodic reaction, $R_{ct,a}$, can increase significantly with the decreasing of cathodic polarization potential. When $R_{ct,a}$ is much larger than $R_{ct,c}$, the cathodic reaction fraction is the determining reaction on the electrode surface. The rate of cathodic reaction depends on the reduction rate of the main depolarizer of dissolved oxygen and H_2O. When the cathodic reaction rate in H_2O reduction fraction is very low, the cathodic dissolution current density, i_c, is approximately equal to the dissolved oxygen dissolution current density, $i_c(O)$. The rate of oxygen reduction is limited to the rate at which oxygen diffuses to the steel surface from the surroundings. For the relationship curves of R_{ct} and polarization potential under various stress levels shown in Fig. 15(b), the presence of the peak under a constant stress level could be attributed to the cathodic reduction reaction of the dissolved oxygen. At the optimum cathodic protection potential, the dissolved oxygen would be used up once it reached the steel surface. Thus, the corrosion rate of the protected Q235B steel at optimum cathodic protection potential would be close to zero. When the cathodic polarization potential decreased further, cathodic reaction in the hydrogen evolution reaction constituted an important proportion and the hydrogen evolution current density, $i_c(H)$, became larger. Synthesizes the $i_c(O)$ and $i_c(H)$, i_c increased dramatically resulting from the impact of $i_c(H)$, leading to a significant decrease in R_{ct} value. When the potential decreased, entering the potential range of -1.0 $V_{Ag/AgCl}$ to -1.2 $V_{Ag/AgCl}$, R_{ct} became very small, indicating that hydrogen evolution reaction and hydrogen permeation had occurred.

Furthermore, when the applied stress level increased, the extra mechanical energy would activate the steel surface and induce a negative shift of corrosion potential and a thickness reduction of diffusion layer at the steel/solution interface. These can be also seen in Fig. 15(b) and Fig. 16, where the optimum cathodic protection potential shifted negatively and R_{ct} decreased with the increasing of applied elastic stress level.

4.4. Implications on the optimization design for ICCP systems

ICCP systems have been used widely to provide cathodic protection for ships and marine structures. During the service life, these structures usually experience various environmental loadings such as wind, waves and current, and the stress caused by machining, operating force, and welding etc. is also unavoidable. It is worth noting that all the stress levels should be within the elastic limit range to meet the safety design of ships and marine structures. It was demonstrated in present study that the elastic stress could enhance corrosion rate of the ships and marine structures and meanwhile could decrease the optimum cathodic protection potential. Therefore, once stress on structural surface changes, it will be necessary to adjust the impressed cathodic current density to achieve the optimum cathodic protection effect, and meanwhile save energy. It is anticipated that some concluding remarks achieved in this study would provide important recommendations that the corrosion enhancement due to the elastic stress on structural surface should be considered in safety design of marine structures, and meanwhile provide an insight into the optimization of cathodic protection system design.

5. CONCLUSIONS

The separate and combined effects of the cathodic protection potential and macro-elastic stress on corrosion behaviors of the Q235B steel in the 3.5% NaCl aqueous solution were investigated. Based on the thermodynamic and kinetic analyses and experimental results, the following conclusions can be obtained:

(1) The increment of surface energy due to the elastic stress is sufficient to cause the negative direction shifted of the corrosion potential and enhance the corrosion rate of Q235B steel significantly.

(2) The relationship curves of R_{ct} and cathodic protection potential under various elastic stress levels were obtained in this study. Based on above relationship curves, the cathodic protection potential for Q235B steel in 3.5% NaCl aqueous solution should not be lower than -1.0 $V_{Ag/AgCl}$, which is the hydrogen evolution potential. When the R_{ct} reaches the peak value, the cathodic protection potential is considered the optimum protection potential.

(3) The novel relationship between the optimum protection potential and elastic stress is nearly linear. The optimum protection potential decreases with the increasing of elastic stress.

(4) In the optimum cathodic protection system design for ships and marine structures, the necessary adjustments of impressed current due to the elastic stress on structural surface should be considered.

ACKNOWLEDGEMENTS

This study was supported by the National Natural Science Foundation of China (Project Nos. 50921001, 51221961 and 51379031), the National Program on Key Basic Research Project of China (Project No. 2011CB013704) and the Project of High Technology Ship of Chinese Ministry of Industry and Information Technology.

References

1. D.A. Jones, *Principles and prevention of corrosion*, Macmillan (1992)
2. M.C. Yan, C. Sun, J. Xu, W. Ke, *Int J Electrochem Sci*, 10 (2015) 1762
3. Z.M. Gao, Y.Y. Liu, F. Lin, L.H. Dang, L.J. Wen, *Int J Electrochem Sci*, 8 (2013) 10446
4. A. Westlake, K. Uppu, A Guideline: *Corrosion Protection of Floating Production and Storage Vessels*, Offshore Technology Conference (2007)
5. R.K. Ren, S. Zhang, X.L. Pang, K.W. Gao, *Electrochim Acta*, 85 (2012) 283
6. R.E. Melchers, J.K. Paik, *Corros Sci*, 51 (2009) 2298
7. J.Q. Yang, Q.Q. Wang, K.S. Guan, *Int J Pres Ves Pip*, 110 (2013) 72
8. Y. Lin, G. Liu, M.-S. Chen, Y.-C. Huang, Z.-G. Chen, X. Ma, Y.-Q. Jiang, J. Li, *Journal of Alloys and Compounds*, 657 (2016) 855
9. X.H. Wang, X.H. Tang, L.W. Wang, C. Wang, W.Q. Zhou, *J Nat Gas Sci Eng*, 21 (2014) 474
10. X.H. Wang, X.H. Tang, L.W. Wang, C. Wang, Z.Z. Guo, *Int J Electrochem Sci*, 9 (2014) 4574
11. K. Gao, D. Li, X. Pang, S. Yang, *Corros Sci*, 52 (2010) 3428
12. B.T. Lu, J.L. Luo, P.R. Norton, H.Y. Ma, *Acta Mater*, 57 (2009) 41
13. J. Liu, Z. Jiang, S. Tian, Q. Huang, Y. Liu, *Journal of Nuclear Materials*, (2015).
14. S. Zhang, X.L. Pang, Y.B. Wang, K.W. Gao, *Corros Sci*, 75 (2013) 293
15. E. Gutman, *Mechano-Chemistry and Corrosion Prevention of Metals*, Science Publication, Peking (1989)
16. B. Hirschorn, M.E. Orazem, B. Tribollet, V. Vivier, I. Frateur, M. Musiani, *Electrochim Acta*, 55 (2010) 6218
17. J. Bisquert, G. Garcia-Belmonte, P. Bueno, E. Longo, L.O.S. Bulhoes, *J Electroanal Chem*, 452 (1998) 229
18. M.R.S. Abouzari, F. Berkemeier, G. Schmitz, D. Wilmer, *Solid State Ionics*, 180 (2009) 922
19. P. Zoltowski, *J Electroanal Chem*, 443 (1998) 149
20. J.B. Jorcin, M.E. Orazem, N. Pebere, B. Tribollet, *Electrochim Acta*, 51 (2006) 1473
21. G.J. Brug, A.L.G. Vandeneeden, M. Sluytersrehbach, J.H. Sluyters, *J Electroanal Chem*, 176 (1984) 275
22. R.N. Deo, N. Birbilis, J.P. Cull, *Corros Sci*, 80 (2014) 339
23. S.P. Harrington, T.M. Devine, *J Electrochem Soc*, 156 (2009) C154
24. C.H. Hsu, F. Mansfeld, *Corrosion*, 57 (2001) 747
25. F.S. Cui, F.J. Presuel-Moreno, R.G. Kelly, *Corros Sci*, 47 (2005) 2987
26. S.P. Harrington, T.M. Devine, *J Electrochem Soc*, 155 (2008) C381
27. A. Collazo, M. Izquierdo, X.R. Novoa, C. Perez, *Electrochim Acta*, 52 (2007) 7513
28. A.J. Bard, L.R. Faulkner, *Electrochemical Methods, 2nd ed*, Wiley, New York (2001)
29. E.M. Gutman, *Mechanochemistry of materials*, Cambridge Int Science Publishing, Cambridge (1998)